Revisiting the paleomagnetism of Muong Nong layered tektites: Implications for their formation process

J. Gattacceca, Pierre Rochette, Yoann Quesnel, Sounthone Singsoupho

METEORITICS & PLANETARY SCIENCE

Revisiting the paleomagnetism of Muong Nong layered tektites: implications for their formation process

Journal:	*Meteoritics & Planetary Science*
Manuscript ID	MAPS-3583
Manuscript Type:	Article
Date Submitted by the Author:	20-Apr-2021
Complete List of Authors:	Gattacceca, Jérôme; CEREGE, Rochette, Pierre; Aix Marseille University CNRS, CEREGE Quesnel, Yoann; Aix-Marseille University, CEREGE Singsoupho, Sounthone; National University of Laos, Department of Physics, Faculty of Natural Sciences
Keywords:	Muong Nong tektite, magnetic properties, Paleomagnetism, Australasian < Tektite(s)

Revisiting the paleomagnetism of Muong Nong layered tektites: implications for their formation process

Jérôme Gattacceca[1], Pierre Rochette[1], Yoann Quesnel[1], Sounthone Singsoupho[2]

[1]CNRS, Aix-Marseille Univ, IRD, INRAE, Aix-en-Provence, France

[2]Department of Physics, Faculty of Natural Sciences, National University of Laos, Vientiane, Laos

Abstract

Among Australasian tektites, the so-called Muong Nong tektites stand out for their peculiar layering and blocky aspect. Although the source crater for the Australasian tektites is not known, Muong Nong tektites are generally considered as a relatively proximal ejecta. The mechanism responsible for the formation of the layering has been a matter of debate. In this work, we revisit the paleomagnetism of Muong Nong tektites. They retain a thermoremanent magnetization acquired during cooling below 585°C in the presence of the ambient geomagnetic field, and carried magnetite in most samples, although at least one sample containing metallic iron was detected. The inclination of the paleomagnetic direction with respect to the layering plane clusters around 18±12°, compatible with the inclination of the geomagnetic field for this latitude at the time of impact. This indicates that the layering of the Muong Nong tektites was sub-horizontal while they were cooling below 585°C. The preferred scenario for the formation of the layering of layered tektite is therefore by horizontal shear in pools or sheets of molten material.

1. Introduction

Tektites are glassy bodies formed by high-temperature melting of target rocks during hypervelocity impacts at the surface of the Earth, and spread over extensive strewnfields (Glass, 1990). Five tektite fields are known: Australasian tektites, belizites, moldavites, ivoirites, North-American tektites, by order of increasing age (Koeberl, 1994; Rochette et al., 2021). All can be associated to a known impact crater, except Australasian tektites whose source is yet not firmly identified, although it has been recently proposed to be hidden under a volcanic plateau in Southern Laos (Sieh et al., 2020). This is surprising in view of their relatively young age of 788±3 ka (Jourdan et al., 2019), the assumed large diameter of the putative crater and extensive spread over at least 180 million km^2 (28% of the surface of the Earth) when including microtektites found in deep sea sediments and Antarctica (Folco et al., 2008; Di Vincenzo al., 2021). A source crater located in Indochina is favored by most authors based on tektite and microtektite distribution (Glass and Pizzuto, 1994; Glass and Koeberl, 2006), despite alternative locations proposed in Northern China (Mizera et al., 2016). However, such a crater has not been confirmed so far. In the absence of crater, competing hypotheses of formation by multiple km-sized craters (Wasson, 1991), or airburst without the need for an impact crater have emerged for the Australasian tektites (e.g., Barnes, 1963; Wasson, 2003). Besides the Australasian tektite case, this debate has far-reaching implications for the understanding of the possible risk and environmental effects associated with large airbursts (e.g., Cavosie and Koeberl, 2019).

Of particular interest in this debate are the Muong-Nong tektites, a sub-category of Australasian tektites characterized by their larger size (up to above 20 kg), blocky aspect without the typical splashforms attesting solidification during flight, and marked layering with adjacent dark and light layers showing differences in chemical composition (Koeberl, 1992). These objects, also

called simply "layered tektites" were named after the town in Laos where they were first identified (Lacroix, 1935). They are found in abundance over an area of ~1000 km radius in East Thailand, South Central Vietnam and Laos (e.g., Barnes, 1971; Koeberl, 1992; Fiske et al., 1999; Schnetzler, 1992; Schnetzler and Mc Hone, 1996; Wasson et al. 1995; Fiske et al. 1999). Layering was proposed to be formed by differential flow of melt with different viscosities in a melt sheet, melt pools or melt puddles along gently inclined surfaces (e.g., Barnes and Pitakpaivan, 1962; Barnes, 1963; Wasson et al., 2003). Geochemistry favors a formation from an ejected inhomogeneous melt flowing after reaching the surface (e.g., Koeberl, 1992). But other models, such as stretching in flight and/or deformation during landing of large masses of molten material have been proposed (Fiske, 1996). Muong Nong tektites are also characterized, with respect to standard splashform australasites, by 1) a higher volatile content (water, noble gases, etc., see Beran and Koeberl 1997; Koeberl, 1992; Mizote et al., 2003), 2) pressure of gas bubbles within the atmospheric range, while splashforms bubble pressure estimates suggests solidification outside the atmosphere (Mizote et al., 2003; Žák et al., 2019), 3) preservation of crystalline inclusions of coesite, cristobalite, zircon, magnetite (Glass and Barlow, 1979; Kleinman, 1969; Krizova et al., 2019; Cavosie et al., 2018; Masotta et al. 2020) indicative of lower peak temperatures.

Models of layering formation by flow in a melt pool or melt sheet (formed either by fallout of liquid ejecta from an impact, or by in situ melting by an airburst) all require that the layering of Muong Nong tektites was sub horizontal during cooling in the Earth magnetic field. Therefore, the angle between layering and natural remanent magnetization (NRM), should be close to the expected inclination of the geomagnetic field at that time, i.e. 28° for a site at latitude 15°N. In this work, following the pioneering study of de Gasparis et al. (1975), we revisited Muong-Nong tektite paleomagnetism to bring further constraints to their original position at the surface during cooling. Indeed, the work by de Gasparis (1973) and de Gasparis et al. (1975) was

focused primarily on the paleointensity of the magnetic field recorded by the tektites, with the objective of determining if tektites were of lunar or terrestrial origin, an active debate at that time. The directional data were only briefly mentioned and discussed, and it was John Wasson who wrote "*I suggest that the remanence should be measured again…*" (Wasson, 2003), and initiated this second study of Muong Nong tektites paleomagnetism.

2. Samples

Tektites are usually characterized by a purely paramagnetic behavior (Rochette et al. 2015, 2019), not adapted for paleomagnetic investigations that require at least 10 ppm of ferromagnetic inclusions such as magnetite or metal. However, it appears that Muong Nong tektites contain a significant amount of such inclusions (Kleinman et al., 1969; Glass and Barlow, 1979; Rochette et al., 2015), making them suitable for a paleomagnetic study (de Gasparis et al., 1975).

We studied 32 samples taken from 18 Muong Nong tektites (Table 1, Figure 1). They were selected for their marked layering (Figure 2). Nine tektites, with label starting with T or TS were selected and characterized by John Wasson. Seven tektites, with label starting with N, were recovered and selected by Pierre Rochette within five collection sites prospected during a field trip in 2019 around the Muong Nong locality in Southern Laos. The larger samples were bought directly from villagers who collected them while cultivating their fields, thus ensuring that the coordinates given in Table 1 are reliable. Finally, two samples (MNP1, MNP2) were obtained from a dealer in Thailand. Selection criteria were well-expressed planar unfolded layering (apart from sample N16, see below), large enough size to allow cutting samples of a few cm^3 lacking magnetic soil incrustations that often found in the porous parts of Muong Nong tektites. We encountered a significant number of Muong Nong where folding of layering prevented the definition of a consistent presumed paleo-horizontal plane for the whole tektite.

To document the paleomagnetic signal behavior of such samples, we cut one folded sample (tektite N16) perpendicular to the fold axis, obtaining four subsamples, two from the fold flanks with a ~40° angular difference, and two from the fold hinge.

Field observations consistently show that Muong Nong tektites, when found *in situ*, occur near the contact between the upper yellow sandy soil formation and an underlying more consolidated red formation rich in lateritic gravel (Schneztler and McHone, 1996; Wasson et al., 1995; Tada et al., 2020; Zak et al. 2019, and our own field work in 2019). Previous interpretations in terms of subsequent deposition of the soil (called loess-like or "catastro-loess" by some authors, see review in Mizera et al., 2016) on top of a lateritic surface on which the Muong Nong tektite fell or formed by in situ melting may be too simplistic. In fact, the "loess-like" material is typical of poor podzolic soils commonly found in hilly zones of tropical humid areas. Between this soil and the lateritic formation, a stone line (rich in quartz pebbles) is consistently observed. Stone lines are usually interpreted as accumulation of insoluble matter after pedogenetic dissolution. Therefore, the in situ position of tektites may not reflect their deposition position but long term pedogenetic processes. Our prospection around Muong Nong locality showed that most sites producing Muong Nong tektite were lateritic gravels pits dug to provide material for dirt roads. Those pits allowed to clearly observe that the Muong Nong tektites, when recovered in situ, have their layering often but not always presently horizontal, and do not occur as a continuous thin layer. The largest continuous layer we observed (with a maximum thickness of 4 cm) was followed along less than one meter laterally. The largest samples we recovered in situ and bought were 150 and 458 g, respectively.

3. Methods

After initial measurement of their bulk natural remanent magnetization (NRM), samples were cut into mutually-oriented subsamples using a wire saw cooled with water. Sample size was

chosen based on the initial NRM measurement to aim for a NRM of at least 10^{-6} Am^2 allowing reliable remanence measurements. Cutting was also aimed at removing the external, weathered part of the tektites, with particular attention to soil incrustations that may be highly magnetic compared to the bulk tektite glass. Additional cleaning was performed using a non magnetic metallic needle, and for some samples with an additional treatment with ethanolamine thioglycolate (EATG) to dissolve remaining adhering terrestrial oxihydroxides. An oriented thin slice was cut from most sample to better define the layering (Figure 2).

Magnetic measurements were performed at CEREGE. The magnetic susceptibility was measured using a MFK1 kappabridge from Agico. Hysteresis properties were measured with a Princeton Micromag vibrating sample magnetometer with a maximum applied field of 1T and a moment sensitivity of ~10^{-8} Am^2. Magnetic remanence was measured with a SQUID magnetometer (2G Enterprises, model 755R, with noise level of 10^{-11} Am^2), except for the initial NRM of large bulk specimens that was measured with a spinner magnetometer (Minispin model from Molspin). Stepwise alternating field (AF) and thermal demagnetization were used to characterize the NRM. AF demagnetization was performed using the in-line three-axis demagnetization of the 2G magnetometer, or off-line by three-axis demagnetization with a LDA5 AF demagnetizer from Agico. Thermal demagnetization was performed with a zero-field oven from ASC. Saturation isothermal remanent magnetization (sIRM) was imparted in a field of 3 T with MMPM9 pulse magnetizer. Anhysteretic remanent magnetization was imparted using the LDA5AF instrument. Magnetization components were computed from NRM demagnetization data by principal component analysis (Kirschvink, 1980), using the Paleomac software (Cogné, 2003).

4. Intrinsic magnetic properties

The intrinsic magnetic properties of the 18 studied Muong Nong tektites, shown in Table 2, can be compared to previous results for Australasian tektites that are mostly paramagnetic with only traces of ferromagnetic inclusions below 1 ppm (see review in Rochette et al., 2015). The average susceptibility for the studied Muong Nong tektites (94.1±17.4 10-9 m3/kg, n=18) is higher than the average for Australasian tektites of 82±10 10-9 m^3/kg, n=152 (Rochette et al., 2015). Similarly, the average saturation remanence (sIRM) of our sample set is 5.20±3.30×10-5 Am2/kg, higher than what is observed in the general Australasian tektite population (≤4×10-6 Am2/kg in Rochette et al., 2015).

Hysteresis properties were measured for subsamples of the six tektites with magnetic susceptibility significantly higher than the average value of 94.1×10^{-9} m^3/kg. All cycles (corrected for the high-field susceptibility computed over the interval 0.8-1 T) are typical of pseudo-single domain magnetite, with the exception of sample T428 that has a hysteresis loop with low B_C, high B_{CR}/B_C and curvature up to 0.7 T (Figure 3A), typical of the presence of multidomain metallic iron as observed in iron metal-bearing meteorites (e.g., Gattacceca et al., 2014). The saturation magnetization (M_S) in magnetite-bearing samples ranges from 8.0×10^{-4} to 1.66×10^{-2} Am^2/kg, indicating a magnetite content in the 8.7 ppm to 180 pm range. The ratios M_{RS}/M_S and B_{CR}/B_C indicate that the magnetite grains are in the pseudo-single domain state (Dunlop, 2002), i.e. in the 80-200 nm size range for equant grains (Muxworthy and Williams, 2015). The M_S value of sample T428 suggests the presence of 58 ppm of metallic iron whose multidomain behavior indicates a grain size above 100 nm. There is no indication of the presence of superparamagnetic grains (Figure 3B).

Thermal demagnetization of the NRM shows a sharp decrease in magnetization at temperatures in the 570-580°C range (Figure 4A), suggesting that the main remanence carrying mineral is magnetite that has a Curie temperature of 585°C. Sample T428, whose main magnetic carrier is metal was not demagnetized thermally by lack of available material.

Demagnetization of sIRM by AF (Figure 4B) shows coercivity spectra in agreement with pseudo-single domain magnetite, with median destructive fields of 21±8 mT. The median destructive field of ARM is 31±9 mT. After AF demagnetization of 100 mT, less than 10% of the sIRM is left in 14 out of 17 tektites (Table 1). Only 3 samples stand out with higher residual IRM after AF demagnetization of 100 mT: T428 (24 %) whose hysteresis properties suggest that it contains metal instead of magnetite, T490 (23%), and N19 (18%). We have no hysteresis data for T490 and N19, but a sample of T490 was demagnetized thermally and shows a unblocking temperature spectrum that is different from the other tektites, with a marked decrease of NRM starting at 490°C rather than 560°C (Figure 4A). This may evidence the presence of metal that is being destroyed rather than demagnetized during the thermal treatment.

5. Paleomagnetism

All paleomagnetic results are summarized in Table 3.

5.1. Tektites affected by lightning-generated magnetic fields

The NRM intensities span 4 orders of magnitude, ranging from 10^{-7} to 10^{-3} Am^2/kg. This is in contrast with the more restricted range of 10^{-7} to 10^{-5} Am^2/kg obtained by de Gasparis et al. (1975). NRM/sIRM ratios of the ten samples with highest NRM are close to, or exceeds 0.1, suggesting that these tektites were exposed to a strong field at some point in their history. This is confirmed by the more refined comparison of AF demagnetization data of NRM and sIRM (Figure 5), using the so-called REM' approach (Verrier and Rochette, 2002; Gattacceca and Rochette, 2004). While most samples have REM' values below 0.1, five samples with strong NRM/sIRM have REM' values well above 0.1 over the whole upper range of their coercivity spectrum (samples N03A, N03B, N17, N20A, T419). It is noteworthy that the REM' values of

these samples are below 0.1 for AF fields below 5-10 mT, evidencing relaxation of their strong field magnetization over time.

The orthogonal projection plots of AF and thermal demagnetization data for sample N17 are shown in Figure 6. The other samples with strong NRM and strong REM' show an identical behavior and are not shown. The orthogonal plot for the AF demagnetization data does not show the curvature typical of exposure to hand magnets, a bad habit that is deeply encroached in the meteorite hunters and collectors (see e.g., Gattacceca et al., 2014). Moreover, the REM' values above 0.1 extends up to 100 mT, setting a lower limit for the strong field responsible for the magnetization (Verrier and Rochette, 2002). In view of the original sample size (above 36 g and up to 275 g), such strong and large magnetic fields if artificial, would only be generated by very large rare earth magnets or electromagnets, not available on the field. Therefore, remagnetization by an artificial magnetic field seems highly improbable. The best explanation to account for their strong NRM is remagnetization by lightning strikes. Such phenomenon is well-known in paleomagnetic studies and result in demagnetization diagrams and NRM/sIRM ratios similar to what we observed here (e.g., Verrier and Rochette, 2002). For samples that have been at the surface or subsurface for ~ 0.8 Myr in a tropical climatic setting, such remagnetization can indeed be expected. Lightning may have occurred any time between the present and 0.8 Ma, thus accounting for the viscous decay of the lower coercivity IRM. These samples cannot be used for the main purpose of our work that require preservation of the original magnetization of the tektites.

Two samples, MNP1 and N20B, have high NRM/sIRM ratio (6.01×10^{-2} and 1.14×10^{-1}) and two components of magnetization (Figure 6). But high REM' > 0.1 are restricted to the lower coercivity component in these two samples: although the low coercivity component was acquired in a strong magnetic field of ~20-40 mT, the high coercivity component is not a strong field magnetization and is discussed further.

5.2. Tektite with folded layering

The four subsamples originating from the tektite sample that was selected for its folded layering (N16) were thermally demagnetized. They all provided a medium temperature (MT) component isolated between ~180°C and ~550°C, and a high temperature component (HT) isolated between ~550°C and 580°C (Figure 6). Both components do not pass a fold test at the 95% confidence level (McElhinny, 1964). We also tested stepwise unfolding of the four direction, and the maximum grouping is obtained for zero unfolding. This means that the magnetization was acquired after the layering was in its present folded state. The MT (resp. HT) directions are similar for the four sub-samples, with a Fisher precision parameter of 35 (resp. 69). The mean MT and HT directions differ by 22.5° and are distinct at the 99% confidence level using the statistical test of McFadden and McElhinny (1990). The negative fold test indicates that folding of the layering occurred at temperature higher than 585°C, in agreement with a glass transition temperature of about 700°C in tektites indicating that the glass ceases to be plastic below this temperature (Arnd and Rombach, 1976; Wilding et al. 1996).

5.3. Tektites with planar layering

Discarding the six tektites (10 sub-samples) that were affected by lighting-induced magnetic fields, the average NRM is 1.52×10^{-6} Am^2/kg, and the median NRM is 7.48×10^{-7} Am^2/kg (n=23 samples). The observed range (5×10^{-8} to 4×10^{-6} Am^2/kg) agrees with the observations of de Gasparis et al. (1975). The demagnetization data are presented in Figure 6. Origin-trending high-temperature (HT) and high coercivity (HC) components could be isolated in all samples. All samples have relatively well-defined paleomagnetic directions with an average maximum angular deviation (MAD, as defined by Kirschvink, 1980) of 9.8±6.3°. The HT component is

unblocked up to 580°C (Figure 4A). The HC component is unblocked up to alternating fields between 50 mT and above 100 mT (Figure 4C), depending on the coercivity spectrum of the samples (Figure 4B). These components are similar in direction among mutually oriented samples of the same tektite. The average angular difference between HT and HC components for mutually oriented samples is 15°, which can be attributed to orientation uncertainties and to the uncertainties on the direction of the magnetization components themselves as reflected by their MAD. The HT/HC components are therefore considered as characteristic remanent magnetizations (ChRM). The paleomagnetic declination is meaningless because samples were recovered as loose non oriented blocks. Therefore, only the absolute value of the inclination, computed with respect to the petrographic layering plane, has a meaning and is given in Table 3. A number of tektites also display a medium temperature (MT), medium coercivity (MC) component of magnetization. The MT components are typically unblocked up 540-560°C, while the MC components are unblocked up to 15-20 mT (Figure 6).

During thermal demagnetization, the NRM is unblocked up to the Curie temperature of pure magnetite (Figure 4A), except for sample T490 whose NRM is fully unblocked at 570°C, but as discussed above, this sample may have metal instead of magnetite as magnetic carrier. This indicates that the magnetization is likely of thermoremanent origin, and was acquired upon cooling from a temperature above 585°C. The REM' ratios, integrated over the HC component, are in the range of $\sim 2\ 10^{-2}$ typical of a thermoremanence in the geomagnetic field (Gattacceca and Rochette, 2004). Therefore, these tektites were magnetized while in a fixed position with respect to the ambient magnetic field. In particular, this precludes that the samples were in flight (spinning) while they were cooling below 585°C. This cooling phase must have taken place with the tektites in a fixed position on the ground at least between 585°C and 100-200°C (the lower bound of the unblocking temperature spectra). However, 7 out of 12 samples show two components of magnetization, with a cut-off temperature in the 540-560°C range. This suggests

a one-step displacement of the tektite while cooling below this temperature. This displacement had to take place in a single phase and quickly (relative to the cooling time in the 585-500°C range) since the two components of magnetization (MT and HT) are well-defined, precluding progressive movement during cooling. Tektite TS6 shows a more complex demagnetization with three components of magnetization unblocked over the intervals 280-520°C, 520°C-575°C, and 575-580°C respectively. This suggest a more complex movement of this tektite during cooling. When several components of magnetization are present, we consider the highest temperature (and highest coercivity) component as the most representative of the original position of the tektite layering, since later movements will only disturb the original orientation. Our interpretation of the two-component magnetizations is implicitly based on the scheme of two successive pTRM. A more complex possibility may be envisioned, with a part of the magnetization being a chemical remanent magnetization due to the growth of magnetite grains through the circa 20 nm blocking size by diffusion in the glass. But the absence of evidence for superparamagnetic grains in the hysteresis properties (figure 3B) argues against such a scenario.

5.4. Paleomagnetic inclination distribution

The distribution of the ChRM inclination with respect to the layering plane is given in Figure 7. When both thermal and AF demagnetization were available, we use the average inclination. For the tektites that had two components of magnetization, we use the HC/HT component that we consider more representative of the original tektite position, as discussed above. We included the 9 inclination values obtained by de Gasparis et al. (1975), eight using AF demagnetization, and one using thermal demagnetization. The inclination distribution is clearly different from a random distribution, with a bias towards low inclinations. This is especially true if we exclude the seven samples with two component of magnetization that had a more complex surface history during cooling. The three samples with inclinations higher than 50° are all

multicomponent. Excluding these seven samples, the average inclination is 18±12°. (n=15, including the 9 inclination values from de Gasparis et al., 1965)

This low inclination could be accounted for by a strong magnetic anisotropy of this layered material, that would deviate NRM directions toward the layering plane with respect to ambient field during cooling. We tested this hypothesis by measuring the anisotropy of ARM, that has been shown to be a good proxy for the anisotropy of thermoremanent magnetization (Gattacceca and Rochette, 2003). The anisotropy of anhysteretic remanent magnetization (ARM) was approximated by assuming that the hard magnetic direction is perpendicular to the layering plane. ARM was imparted in a AF field of 140 mT and a bias field 100 μT along three orthogonal direction, one of which being perpendicular to the layering plane. The minimum ARM was awlays measured along the direction perpendicular to the layering plane. The average AARM degree, computed as the maximum over the minimum ARM, is P_{ARM} = 1.12±0.07, with a range 1.04-1.26. This would result in an average deviation of the ChRM with respect to the ambient magnetic field of 2°, and a maximum deviation of 4° (considering the average inclination of 18° with respect to the layering plane). This point was also discussed, with similar conclusion by de Gasparis et al. (1975), using IRM anisotropy. In conclusion, magnetic anisotropy cannot be responsible for the shallow inclination distribution.

As a result, the only explanation for a non random distribution of inclinations in Muong Nong tektites is that the layering was sub-horizontal at the time they cooled below 585°C. The average inclination of the geomagnetic field at 0.8 Ma for latitude 15°N is 28°, slightly higher than the average inclination of 18±12° measured in the Muong Nong tektites. The difference is easily accounted for by the paleosecular variation of the magnetic field that can result in deviation of the instantaneous geomagnetic inclination from the average inclination by as much as 15-20° (e.g., Lund; 2018), as well as low data number, uncertainties on the layering plane and imperfect

initial horizontality of this plane. The hypothesis of a post impact cooling of Muong Nong tektites with their layering horizontal on average, is thus confirmed.

6. Implications for the formation of Muong Nong tektites

The confirmation that the Muong Nong tektite layering was sub-horizontal when they cooled below 585°C precludes a scenario in which layering is acquired and frozen during ejection or flight (Fiske, 1996). The sub-horizontal layering is compatible with scenarii in which melt pools or a melt sheet are formed either by an airburst (Wasson, 2003), or by the fallout of ejected liquid material. Horizontal spreading or downslope flow in these melt pools or melt sheets would have then imparted a sub-horizontal layering (e.g., Barnes and Pitakpaivan, 1962; Wasson, 2003). Our results cannot discriminate between these two models (in situ melting by an airburst versus fallout following an impact), although the present-day dominant model is that of an impact, favored for instance by the presence of high pressure phases in Australasian tektites (Cavosie et al., 2018). Moreover, the airburst model does not imply strong horizontal flow and is not clearly able to produce a layering.

The occurrence of a few samples showing evidence of movements occurring during the cooling history, when the tektite was at a temperature of 540-560°C, show that the tektite melt pools or melt sheet may have behaved in a similar way as lava pool, where rotations of already solidified parts are common, resulting in pahoehoe type features.

Although we can roughly estimate the absolute value of the inclination of the geomagnetic field at the time of impact, there is no constraint about its sign. The tektite-forming impact took place at 788±3 ka, shortly before the Brunhes-Matuyama reversal of the geomagnetic field dated at 773 ka (Simon et al., 2019). The inclination of the geomagnetic field was therefore negative at the location of the Muong Nong tektites. As a side result, paleomagnetism may provide a way

to determine the original polarity of the layering of the Muong Nong tektites, as the inclination of the NRM with respect to the layering plane should be negative (i.e., the NRM should be pointing up).

7. Conclusion

Our results show that while some Muong Nong tektites have been remagnetized by strong magnetic fields, likely lighting-generated, a significant fraction retains a thermoremanent magnetization acquired during cooling below 585°C in the presence of the ambient geomagnetic field. This magnetization is carried by magnetite in most samples, although at least one sample containing metallic iron was detected. The study of a sample with a folded layering show that the folding was acquired at temperatures above 585°C. For samples with simple planar layering, the inclination of the paleomagnetic direction with respect to the layering plane is not random and clusters near horizontal, with an average of 18±12°, compatible with the inclination of the geomagnetic field for this latitude at the time of impact. This confirms, based on a more extensive dataset, previous paleomagnetic results (de Gasparis et al., 1975) showing that the layering of the Muong Nong tektites was sub-horizontal while they were cooling below 585°C. Some tektites kept this position at least until they cooled below 100-200°C, while others were affected by movements suggesting a dynamic cooling environment. The preferred scenario for the formation of the layering of layered tektite is therefore by horizontal shear in pools or sheets of molten material. Paleomagnetism also provide a way to determine the polarity of the layering of Muong Nong tektites.

Acknowledgements

This work is dedicated to the memory of John T. Wasson, for his inspiring leadership in the field of meteorite and tektite studies. John suggested the topic of this article to the first author

during a memorable lunch in downtown Casablanca during the Meteoritical Society Meeting in 2014, and provided well-characterized samples for the study.

References

Arndt J., and Rombach N. 1976. Derivation of the thermal history of tektites and lunar glasses from their thermal expansion characteristic. *7th Lunar and Planetary Science Conference*: 1123–1141.

Barnes V.E. 1963. Terrestrial implication of layering, bubble shape and minerals along faults in tektite origin. *Geochimica et Cosmochimica Acta* 28:1267–1271.

Barnes V.E. 1971. Description and origin of large tektite from Thailand. *Chemie der Erde* 30:13–19.

Barnes V.E., and Pitakpaivan K. 1962. Origin of indochinite tektites. *Proceedings of the National Academy of Sciences* 48:947–955.

Beran, A., and Koeberl, C. 1997, Water in tektites and impact glasses by Fourier-transform infrared spectroscopy. *Meteoritics and Planetary Science* 32:211–216.

Cavosie A.J., Timms N.E., Erickson T.M., and Koeberl, C. 2018. New clues from Earth's most elusive impact crater: Evidence of reidite in Australasian tektites from Thailand. *Geology* 46:203–206.

Cavosie A.J., and Koeberl C. 2019. Overestimation of threat from 100 Mt–class airbursts? High-pressure evidence from zircon in Libyan Desert Glass. *Geology* 47:1–4.

Cogné, J.P., 2003. PaleoMac: a Macintosh™ application for treating paleomagnetic data and making plate reconstructions. *Geochemistry Geophysics Geosystems* 4, http://dx.doi.org/10.1029/2001GC000227.

De Gasparis A.A. 1973. Magnetic properties of tektites and impact glasses. Ph.D thesis, University of Pittsburgh, 173 p.

De Gasparis A.A., Fuller M., and Cassidy W. 1975. Natural remanent magnetism of tektites of the Muong-Nong type and its bearing on models of their origin. *Geology* 3:605–607.

Di Vincenzo G., Folco L., Suttle .M D., Brase L., Harvey R. P. 2021. Multi-collector $^{40}Ar/^{39}Ar$ dating of microtektites from microtektites from Transantarctic Mountains (Antarctica): a definitive link with the Australasian tektite/microtektite strewn field. *Geochimica et Cosmochimica Acta* 298:112-130.

Dunlop D. J. 2002. Theory and application of the Day plot (Mrs/Ms versus Hcr/Hc): 1. Theoretical curves and tests using titanomagnetite data. *Journal of Geophysical Research* 107(B3), 2056.

Fiske P. S. 1996. Constraints on the formation of layered tektites from the excavation and analysis of layered tektites from northeast Thailand. *Meteoritics and Planetary Science* 31:42–45.

Fiske P. S., Schnetzler C. C., McHone J., Chanthavaichith K. K., Homsombath I., and Phouthakayalat T. 1999. Layered tektites of Southeast Asia: Field studies in Central Laos and Vietnam. *Meteoritics and Planetary Science* 34:757–762.

Folco L., Rochette P., Perchiazzi N., D'Orazio M., Laurenzi M. A., and Tiepolo M. 2008. Microtektites from Victoria Land Transantarctic Mountains. *Geology*:36, 291–294.

Gattacceca J., Suavet C., Gattacceca J., and Rochette P.2004. Toward a robust normalized magnetic paleointensity method applied to meteorites. *Earth and Planetary Science Letters* 227:377–393.

Gattacceca J., Suavet C., Rochette P., Weiss B. P., Winklhofer M., Uehara M., and Friedrich J. 2014. Metal phases in ordinary chondrites: magnetic hysteresis properties and implications for thermal history. *Meteoritics and Planetary Science* 49:652–676.

Glass, B.P. 1990. Tektites and microtektites: Key facts and inferences. *Tectonophysics* 171:393–404.

Glass B. P., and Barlow R. A. 1979. Mineral inclusions in Muong-Nong-type indochinites - implications concerning parent material and process of formation. *Meteoritics* 14:55–67.

Glass B. P., and Pizzuto J. E. 1994. Geographic variation in Australasian microtektite concentrations: Implications concerning the location and size of the source crater. *Journal of Geophysical Research* 99:19,075–19,081.

Glass B. P., and Koeberl C. 2006. Australasian microtektites and associated impact ejecta in the South China Sea and the Middle Pleistocene supereruption of Toba. *Meteoritics and Planetary Science* 41:305–326.

Jourdan F., Nomade S., Wingate M., Eroglu E., and Deino A. 2019. Ultra-precise age and temperature of formation of the Australasian tektites constrained by $^{40}Ar/^{39}Ar$ analyses. *Meteoritics and Planetary Science* 54: 2573–2591.

Kirschvink, J.L., 1980. The least-squares line and plane and the analysis of palaeomagnetic data. *Geophysical Journal International* 62:699–718.

Kleinmann B. 1969. Magnetite bearing spherules in tektites. *Geochimica et Cosmochimica Acta* 33:1113–1120

Koeberl C. 1992. Geochemistry and origin of Muong Nong-type tektites. *Geochimica et Cosmochimica Acta* 56:1033–1064.

Koeberl C. 1994. Tektite origin by hypervelocity asteroidal or cometary impact. Target rocks, source craters, and mechanisms, *in* Dressler, B.O., Grieve, R.A.F., and Sharpton, V.L., eds., Large Meteorite Impacts and Planetary Evolution: Geological Society of America Special Paper 293, p. 133–152.

Krizova S., Skala R., Halodova P., Zak K., and Ackerman L. 2019. Near end-member shenzhuangite, NiFeS2, found in Muong Nong-type tektites from Laos. *American Mineralogist* 104:1165–1172.

Lacroix, A. 1935. Les tectites sans formes figurées de l'Indochine, *Comptes-Rendus de l'Académie des Sciences Paris* 200:2129–2132.

Lund S. P. 2018. A New View of Long-Term Geomagnetic Field Secular Variation. *Frontiers in Earth Science*, https://doi.org/10.3389/feart.2018.00040

Masotta, M., Peres, S., Folco, L., Mancini, L., Rochette, P., Glass, B. P., Campanale, F., Gueninchault, N., Radica, F., Singsoupho, S., and Navarro, E. 2020. 3D tomographic analysis reveals how coesite is preserved in Muong Nong-type tektites. *Scientific reports* 10, 20608. https://doi.org/10.1038/s41598-020-76727-6.

McElhinny M. W. 1964. Statistical significance of the fold test in palaeomagnetism. *Geophysical Journal International* 8:338–340.

McFadden P. L., and McElhinny M. W. 1990. Classification of the reversal test in palaeomagnetism. *Geophysical Journal International* 103:725–729.

Mizera J., Randa Z., and Kamenik J. 2016. On a possible parent crater for Australasian tektites: Geochemical, isotopic, geographical and other constraints. *Earth-Science Reviews* 154:123–137.

Mizote S., Matsumoto T., Matsuda J., and Koeberl C. 2003. Noble gases in Muong Nong-type tektites and their implications. *Meteoritics and Planetary Science* 38:747–758.

Muxworthy A. R., Williams W. 2015. Critical single-domain grain sizes in elongated iron particles: implications for meteoritic and lunar magnetism. *Geophysical Journal International* 202:578-583.

Rochette P., Gattacceca J., Devouard B., Moustard F., Bezaeva N., Cournède C., and Scaillet B. 2015. Magnetic properties of tektites and other related impact glasses. *Earth and Planetary Science Letters* 432:381–390.

Rochette P., Bezaeva N., Kosterov A., Gattacceca J., Masaitis V., Badyukov D. Giuli G., Lepore G.O., Beck P. 2019. Magnetic Properties and Redox State of Impact Glasses: A Review and New Case Studies from Siberia. *Geosciences* 9 (5), 225

Rochette, P., Beck, P., Braucher, R., Cornec, J., Debaille, V., Devouard, B., Gattacceca, J., Jourdan, F., Moustard, F., Moynier, F., Nomade, S., and Reynard, B. 2021. A new tektite strewn-field and source crater couple discovered in Central America: insights into the tektite generation process and its ubiquity. *Communications Earth & Environment,* in press.

Schnetzler C. C. 1992. Mechanism of Muong Nong-type tektite formation and speculation on the source of Australasian tektites. *Meteoritics* 27:154–165.

Schnetzler C. C., and McHone J. F.1996. Source of Australasian tektites: Investigating possible impact sites in Laos. *Meteoritics and Planetary Science* 31:73–76.

Sieh K., Herrin J., Jicha B., Schonwalder Angel D., James S., Moore D.P., Banerjee P., Wiwegwin W., Sihavong V., Singer B., Chualaowanich T., and Charusiri P. 2020. Australasian impact crater buried under the Bolaven volcanic field, Southern Laos. *Proceedings of the National Academy of Sciences* 117:1346–1353.

Simon Q., Suganuma Y., Okadad M., Hanedad Y., and ASTER Team. 2019. High-resolution 10Be and paleomagnetic recording of the last polarity reversal in the Chiba composite section: Age and dynamics of the Matuyama–Brunhes transition. *Earth and Planetary Science Letters* 519:92–100.

Tada T., Tada R., Chansom P., SOngtham W., Carling P.A., and Tajika E. 2020. In situ occurrence of Muong Nong-type Australasian tektite fragments from the Quaternary deposits near Huai Om, northeastern Thailand. *Progress in Earth and Planetary Science* 66,7.

Verrier V., and Rochette P. 2002. Estimating peak currents at ground lightning impacts using remanent magnetization. *Geophysical Research Letters* 29(18), 1867.

Wasson J. T. 1991. Layered tektites: a multiple impact origin for the Australasian tektites. *Earth and Planetary Science Letters* 102:95–109.

Wasson J. T., Pitakpaivan K., Putthapiban P., Salyapongse S., Thapthimthong B., and McHone J. F. 1995. Field recovery of layered tektites in Northeast Thailand. *Journal of Geophysical Research-Planets* 100:14383–14389.

Wasson J. T. 2003. Large aerial bursts: an important class of terrestrial accretionary events. *Astrobiology* 3:163–79

Wilding M., Webb S., and Dingwell D. B. 1996. Tektite cooling rates: Calorimetric relaxation geospeedometry applied to a natural glass. *Geochimica et Cosmochimica Acta* 60:1099–1103.

Žák K., Skala R., Randa Z., and Mizera J. 2019. A review of volatile compounds in tektites, and carbon content and isotopic composition of moldavite glass. *Meteoritics and Planetary Science* 47:1010–1028.

Captions

Figure 1. Location of studied samples. The coordinates for samples studied in de Gasparis et al. (1973) are from de Gasparis (1971).

Figure 2. Pictures of a selection of studied tektites, before cutting to extract a sample oriented with respect to the layering. For each sample, a picture of a thin slice in transmitted light is shown to highlight the layering.

Figure 3. A) Mass-normalized hysteresis cycles for Muong Nong tektites samples N20A and T428, corrected for the paramagnetic and diamagnetic contribution computed over the 0.8-1 T interval. B) Hysteresis parameters for all measurable samples. Horizontal and vertical lines roughly divide the plot into regions with single domain (SD), pseudo-single domain (PSD), superparamagnetic (SP) and multidomain (MD) behavior. The gray curves represent mixtures of PSD, SD, and MD grains for magnetite (from *Dunlop*, 2002)

Figure 4. A) Evolution of NRM during thermal demagnetization. Sample T420 that was demagnetized by a combination of AF and thermal demagnetization is not shown. Sample T490 that contains metallic iron is indicated. B) Evolution of sIRM during AF demagnetization. The five samples with highest coercivity are indicated. C) Evolution of NRM during AF demagnetization. Samples that were remagnetized by lightning are not shown in figures A and C.

Figure 5. REM' versus AF field for representative samples: magnetized by strong field (N3A), partially magnetized by strong field (MNP1), devoid of strong field magnetization (T490). REM' is the equal to ΔNRM/ΔIRM over successive AF demagnetization steps (see Gattacceca and Rochette, 2004 for lengthy explanations).

Figure 6. Orthogonal plot of demagnetization data for all studied samples not remagnetized by lightning. Among samples remagnetized only lightning, only N17 is shown for example. The demagnetization data are projected on two orthogonal planes: layering plane (solid symbols), and a plane orthogonal to the layering (open symbols). Boxes indicate sub samples from the same tektite. The AF or temperature is indicated from some steps.

Figure 7. Histogram of inclinations of the characteristic remanent magnetization with respect to layering. Samples from this study with a single component of magnetization are highlighted, followed by data from de Gasparis et al. (1975), followed by samples with two components of magnetization (MT/MC and HC/HT). Distribution for an equivalent number of random directions is shown (N=21 for all data, N=14 without the multicomponent samples, N=5 with our single component samples only).

Jérôme Gattacceca
e-mail:gattacceca@cerege.fr

Editor of *MAPS*

Aix-en-Provence, April 19, 2021

Dear Editor,

Please find attached a manuscript called "*Revisiting the paleomagnetism of Muong Nong layered tektites: implications for their formation process*" by myself and co-authors that we would like to submit to *Meteoritics and Planetary Sciences* for the special issue honoring John Wasson.

Indeed, the topic of this study was suggested to us in 2014 by John Wasson who had a long time interest in tektites and in Muong Nong tektites in particular. He also selected the samples for the study. Unfortunately, I was not able to complete the study before he passed away.

The original scope of this paleomagnetic study was to confirm that the layering of Muong Nong tektites was sub-horizontal at the time these glasses were cooling. In addition to this confirmation, that provide constraints on the formation mechanism of these tektites, we provide interesting data about the magnetic mineralogy of this unusual material.

Yours sincerely,

Jérôme Gattacceca

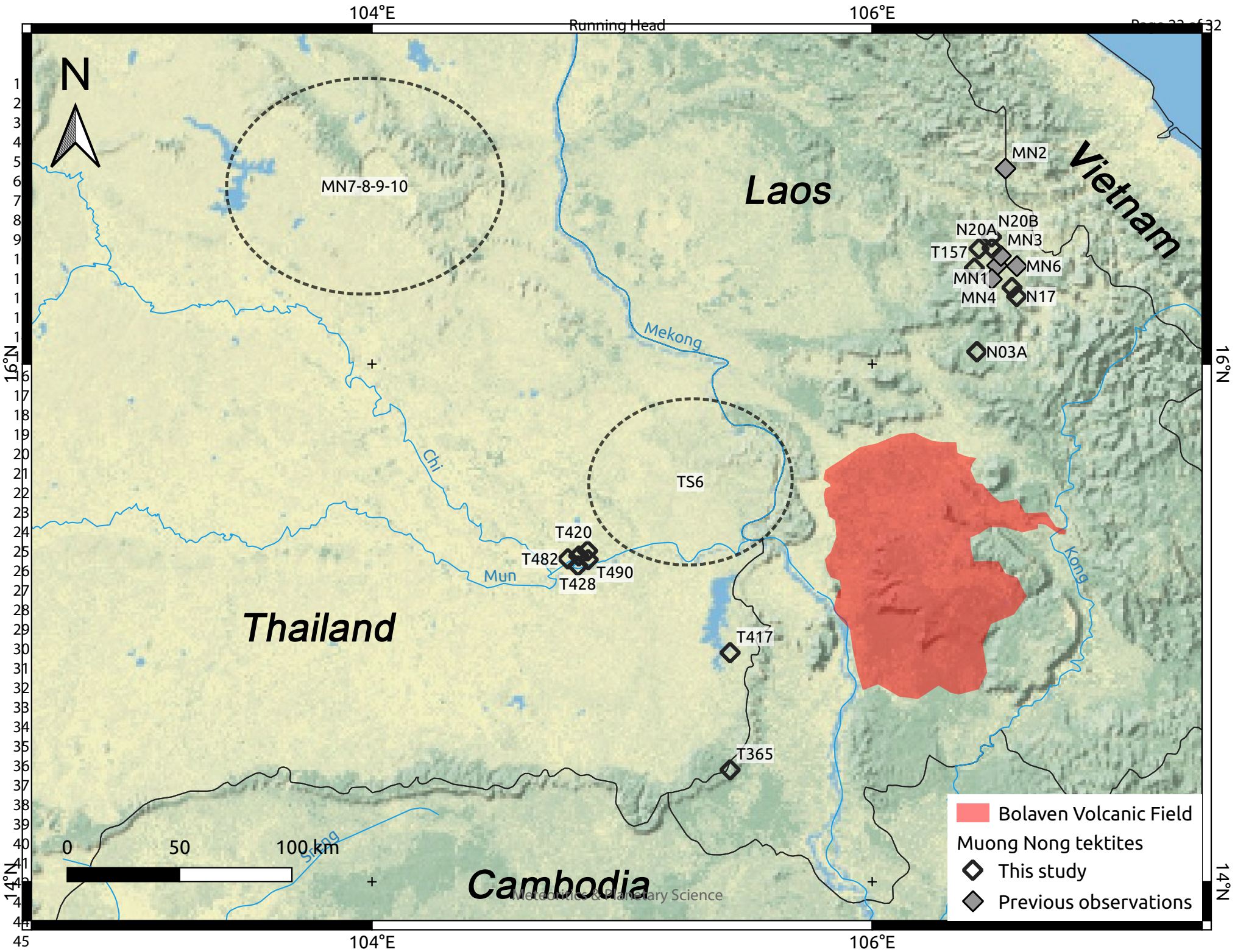

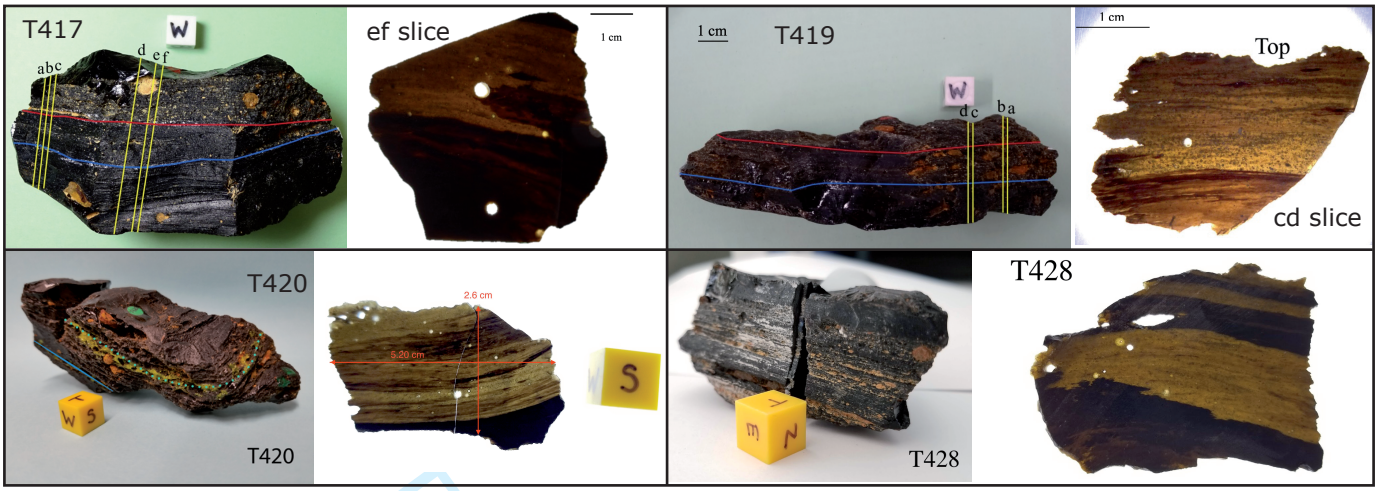

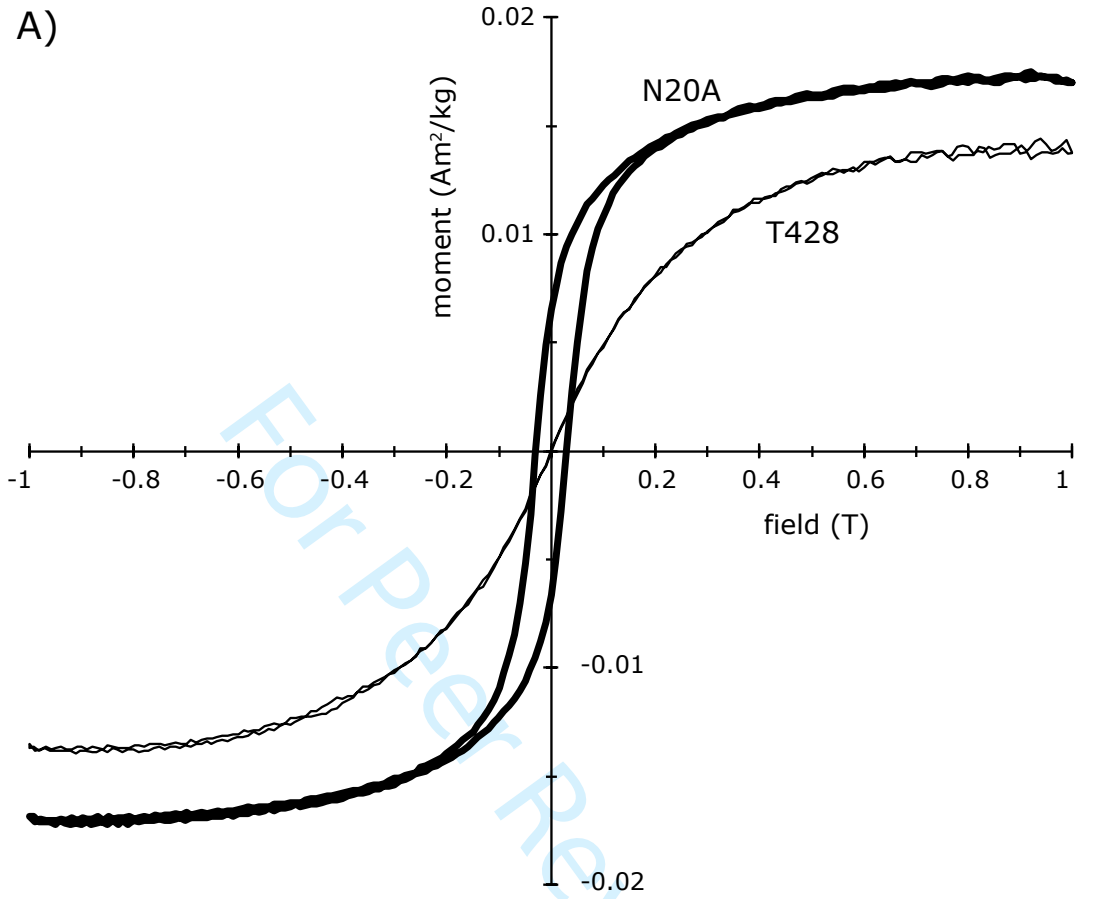

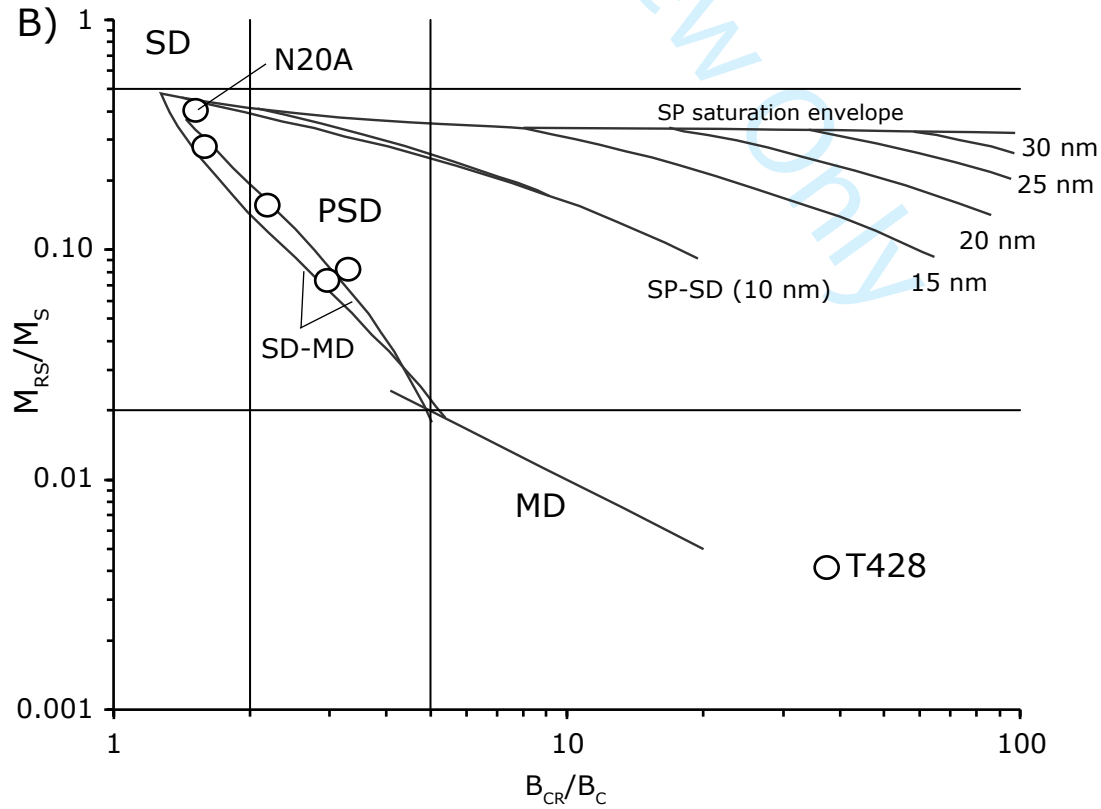

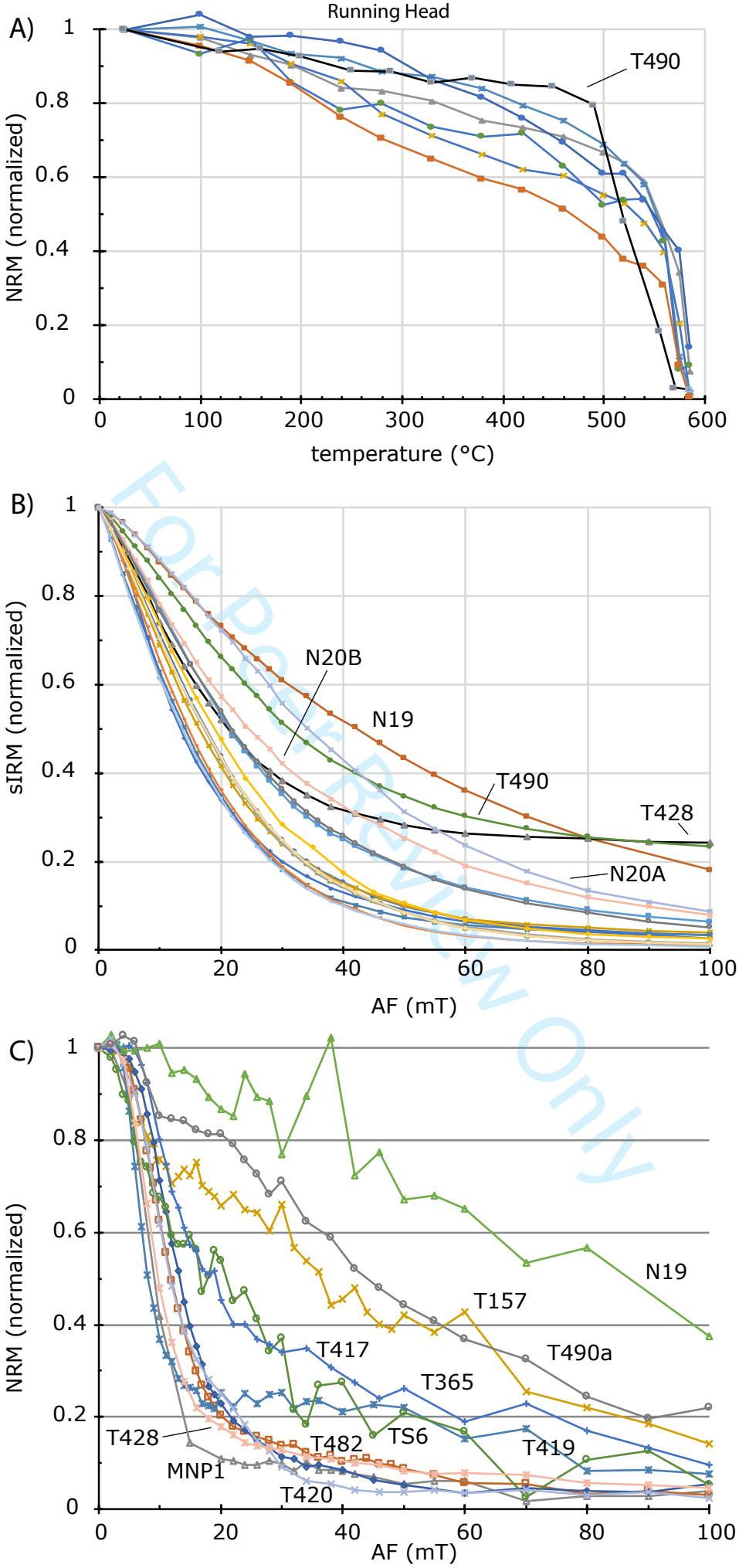

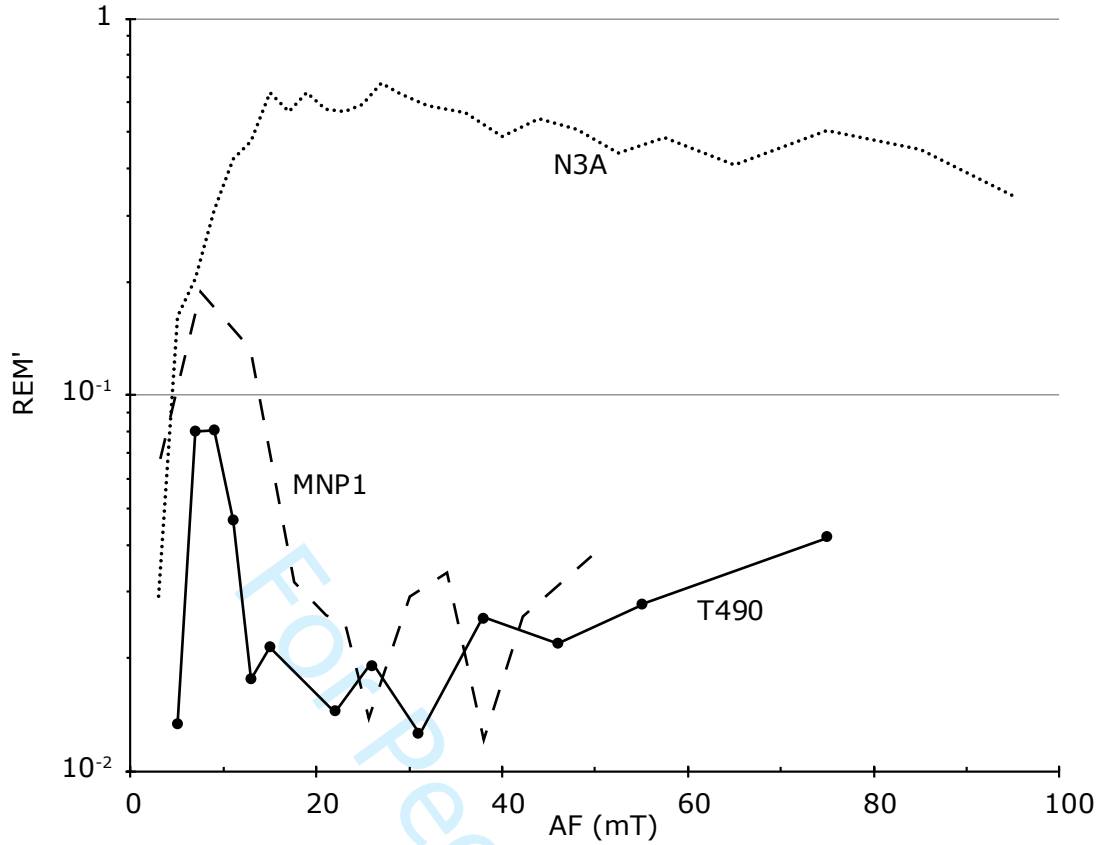

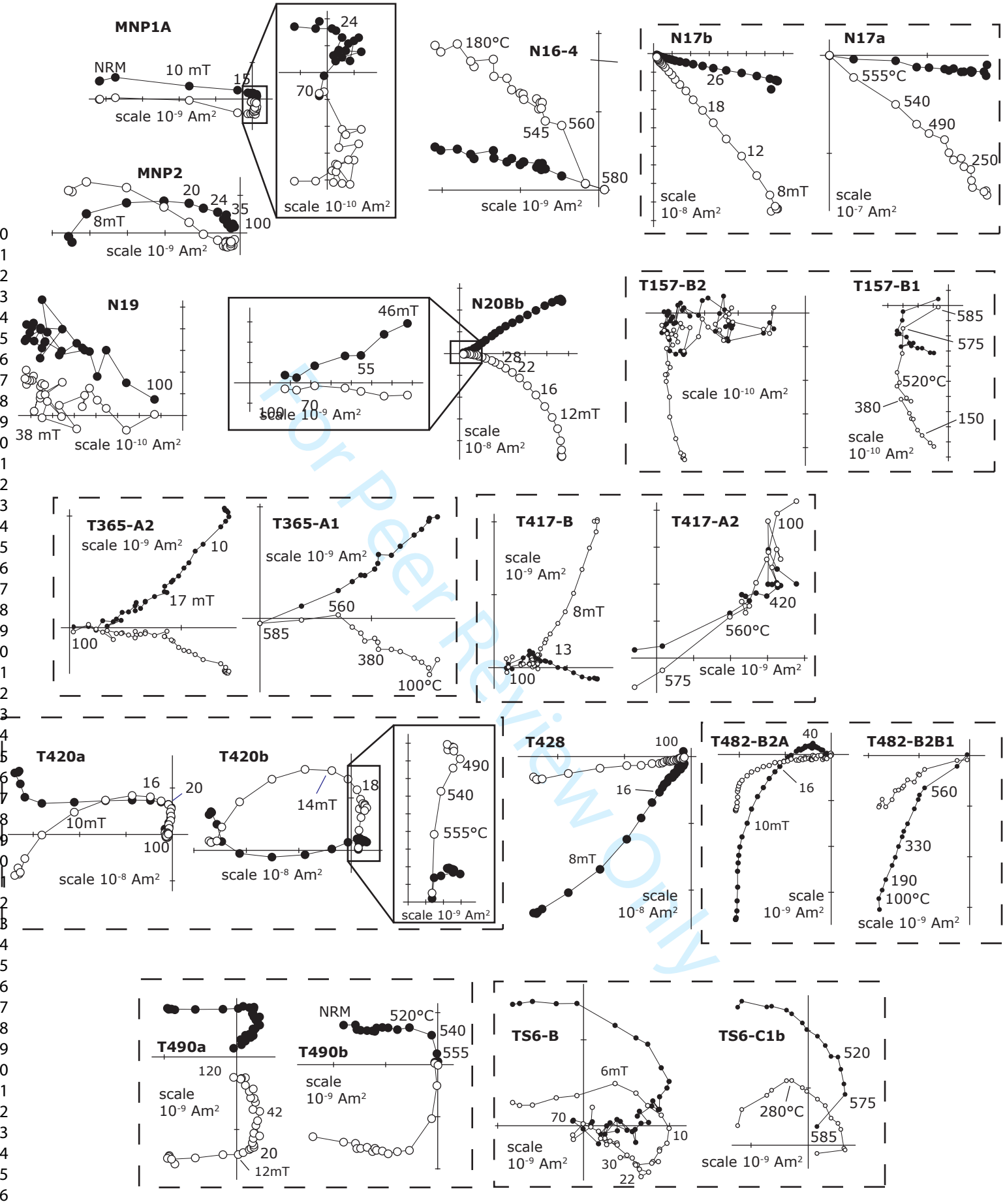

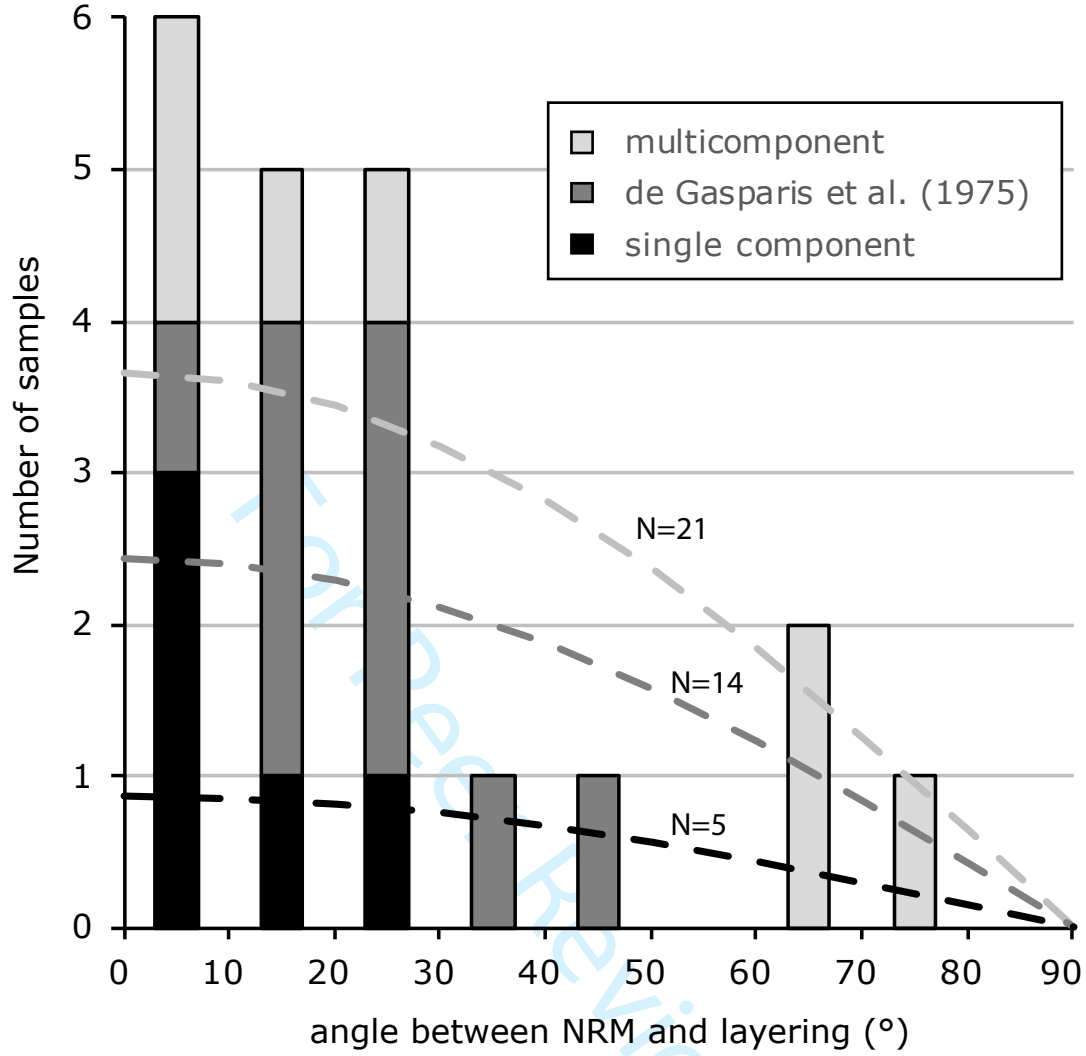

Tables

Table 1: List of studied samples.

sample	mass (g)	latitude N	longitude E	area	collection
MNP1	95			Thailand (?)	CEREGE collection£
MNP2	350			Thailand (?)	CEREGE collection£
N03A	278	16°02'48.72"	106°25'08"	Muong Nong area, Southern Laos	CEREGE collection$
N03B	128	16°02'48.72"	106°25'08"	Muong Nong area, Southern Laos	CEREGE collection$
N16	210	16°17'37.5"	106°33'33.2"	Muong Nong area, Southern Laos	CEREGE collection$
N17	275	16°15'33.5"	106°34'40.4"	Muong Nong area, Southern Laos	CEREGE collection$
N19	36	16°26'32"	106°28'06.3"	Muong Nong area, Southern Laos	CEREGE collection*
N20A	49	16°26'34.5"	106°28'48.7"	Muong Nong area, Southern Laos	CEREGE collection*
N20B	36	16°26'34.5"	106°28'48.7"	Muong Nong area, Southern Laos	CEREGE collection*
TS6	6000			SE of Ubon Ratchathani, Thailand	Smithsonian Institution
T157	179	~16°22'	~106°30'	Muong Nong area, Southern Laos	UCLA collection
T365	322	14°26'0"	105'25'54"	Ban Nong Paen, North East Thailand	UCLA collection
T417	288	14°53'12"	105°25'54"	Ban Huai Sai, North East Thailand	UCLA collection
T419	215	~14°54’	~105°25’	Ban Huai Sai, North East Thailand	UCLA collection
T420	348	~14°54’	~105°25’	Ban Huai Sai, North East Thailand	UCLA collection
T428	127	~14°54’	~105°25’	Ban Huai Sai, North East Thailand	UCLA collection
T482	546	~14°54’	~105°25’	Ban Huai Sai, North East Thailand	UCLA collection
T490	183	~14°54’	~105°25’	Ban Huai Sai, North East Thailand	UCLA collection

*collected in situ, $: bought from villagers, £: bought from a dealer

Table 2: **Hysteresis properties**

sample	mass (g)	M_S (10^{-3} Am^2/kg)	M_{RS} (10^{-3} Am^2/kg)	B_C (mT)	B_{CR} (mT)	χ_{HF} (10^{-9} m^3/kg)	χ (10^{-9} m^3/kg)
N17	0.23	8.3	2.24	27	43	60.1	133
N20A	1.04	16.6	6.47	29.4	45.1	61.1	205
N20B	5 .14	0.8	0.120	16	35	54.4	147
T419	0.74	1	0.080	9	30	81.9	108
T428	1.22	13.1	0.052	0.8	30	54.8	133
TS6	1.92	1.5	0.105	9	27	65.1	106

M_S: saturation magnetization, M_{RS}: saturation remanence, B_C: coercivity, B_{CR}: coercivity of remanence, χ_{HF}: high-field (paramagnetic + diamagnetic) susceptibility, χ: low-field susceptibility.

Table 3. Paleomagnetic results

									HC/HT component				MC/MT component			
sample	sub-sample	method	mass (g)	NRM (Am2/kg)	sIRM (Am2/kg)	MDF ARM (mT)	MDF sIRM (mT)	χ (10^{-9} m^3/kg)	range	n	I (°)	MAD (°)	range	n	I (°)	MAD (°)
MNP1		AF	1.81	2.33×10^{-6}	3.87×10^{-5}	28	17	81.9	24-70 mT	15	73.2	29.3	5-20 mT	4	-7.2	3
MNP2		AF	16.1	2.87×10^{-7}	1.12×10^{-5}	32	19	99.3	16-70 mT	12	-28	9.3				
N03A†	a	AF	9.83	6.52×10^{-6}	1.62×10^{-5}	30	16.5	77.3								
N03B†	a	Th	10.69	3.34×10^{-6}				80.5	330-585 mT	10	51.9	2.6				
N03B†	b	AF	4.65	5.16×10^{-6}	2.17×10^{-5}	13	13	80.5	14-100 mT	19	45.4	1.3				
N16	1	Th	17.9	1.49×10^{-7}				93.6								
N16	2	Th	14.71	5.14×10^{-8}				87.3								
N16	3	Th	14.86	6.93×10^{-8}				86.9								
N16	4	Th	11.58	2.46×10^{-7}				87.7								
N17†	a	Th	10.75	1.97×10^{-5}				83.5	250-585°C	12	38.6	2.6				
N17†	b	AF	5.85	1.85×10^{-5}	1.28×10^{-4}	24	15	83.5	10-80mT	20	48.8	0.9				
N19		AF	10.47	7.01×10^{-8}	8.26×10^{-6}	26	42	88.6	4-120 mT	23	16.9	21.3				
N20A†	a	AF	6.98	5.79×10^{-4}	1.91×10^{-3}	40	34	147.3	8-70 mT	20	15.6	1.4				
N20A†	b	Th	6.14	9.27×10^{-4}				147.3	100-585 °C	16	15.1	1.1				
N20B	b	AF	5.15	1.37×10^{-5}	1.20×10^{-4}	43	24	86.6	46-100 mT	7	3.3	5.5				
T157	B1	Th	5.89	1.68×10^{-7}				80.6	575-585 °C	2	26	8.9	540-575	3	65.6	4.3
T157	B2	AF	2.84	2.03×10^{-7}	1.41×10^{-4}	32	21	81.3	13-90 mT	27	9.5	21.7	5-12 mT	10	65.9	9.1
T365	A1	Th	0.44	4.24×10^{-6}				83.4	560-585 °C	4	-4.5	2.9	100-560 °C	15	23.5	5.5
T365	A2	AF	0.40	4.46×10^{-6}	7.61×10^{-5}	30	22	84.5	20-100 mT	16	5	10.7	8-17 mT	9	18.6	4.9
T417	A2	Th	2.90	2.08×10^{-7}				89.9	540-580 °C	4	-32.6	2.9	240-540 °C	10	-58.2	19.8
T417	B2	AF	3.26	7.48×10^{-7}	3.50×10^{-5}	29	17	88.1	15-100 mT	22	-7.3	7.5	5-15 mT	11	-61.9	3.3
T419†	B3b	Th	0.40	5.29×10^{-6}				108.3	500-585 °C	6	57.7	3.2				
T419†	B2	AF	0.74	6.97×10^{-6}	7.23×10^{-5}	28	17	96.6	12-100 mT	25	58.6	3.1				
T420	a	AF	11.12	3.29×10^{-6}	8.05×10^{-5}	31	14	94.8	22-120 mT	18	-46.4	6.3	8-20 mT	6	5.1	8.4
T420	b	Th£	14.26	1.96×10^{-6}				96.1	250-570 °C¥	11	-76.7	6.3				
T428		AF	13.33	2.51×10^{-6}	5.59×10^{-5}	50	21	132.7	22-100 mT	18	8.5	7.3				
T482	B2B1	Th	1.11	3.29×10^{-6}				94.6	100-585°C	18	15.7	8				
T482	B2A	AF	1.55	2.80×10^{-6}	5.23×10^{-5}	28	17	93.5	34-90 mT	15	2.2	19.7				
T490	a	AF	14.41	1.26×10^{-7}	8.54×10^{-6}	38	31	84.9	18-120 mT	20	64.4	9.6	2-14 mT	7	3.6	2.4
T490	b	Th	16.63	1.84×10^{-7}				81.2	540-585 °C	4	63.6	4.1	25-520 °C	12	-8	9
TS6	C1b	Th	1.96	1.39×10^{-6}				103.1	560-585 °C	4	-5.3	6.1	280-560 °C	10	-37.5	7.6
TS6	B	AF	1.90	8.74×10^{-7}	1.16×10^{-4}	18	13	106.5	22-100 mT	17	32.5	20.6	9-20 mT	11	-44.6	17

†: remagnetized by lightning; £: demagnetized by AF to 18 mT before thermal demagnetization. MDF: median destructive field, I: angle between the magnetization component and the layering plane, MAD: maximum angular deviation, n: numbers of steps used in the computation of the magnetization component.